JBC RESEARCH ARTICLE

Structural and functional analyses of the *Porphyromonas gingivalis* type IX secretion system PorN protein

Received for publication, October 15, 2021, and in revised form, January 15, 2022 Published, Papers in Press, January 21, 2022,
https://doi.org/10.1016/j.jbc.2022.101618

Olivier Fuchsbauer[1,2,‡], **Ignacio Lunar Silva**[3,‡], **Eric Cascales**[3], **Alain Roussel**[1,2], **and Philippe Leone**[1,2,*]

From the [1]*Architecture et Fonction des Macromolécules Biologiques, Aix-Marseille Université, and* [2]*Architecture et Fonction des Macromolécules Biologiques, Centre National de la Recherche Scientifique, UMR 7257, Marseille, France;* [3]*Laboratoire d'Ingénierie des Systèmes Macromoléculaires, Institut de Microbiologie, Bioénergies et Biotechnologie, Aix-Marseille Université - Centre National de la Recherche Scientifique (UMR7255), Marseille Cedex 20, France*

Edited by Karen Fleming

***Porphyromonas gingivalis*, the major human pathogen bacterium associated with periodontal diseases, secretes virulence factors through the *Bacteroidetes*-specific type IX secretion system (T9SS). Effector proteins of the T9SS are recognized by the complex via their conserved C-terminal domains (CTDs). Among the 18 proteins essential for T9SS function in *P. gingivalis*, PorN is a periplasmic protein that forms large ring-shaped structures in association with the PorK outer membrane lipoprotein. PorN also mediates contacts with the PorM subunit of the PorLM energetic module, and with the effector's CTD. However, no information is available on the PorN structure and on the implication of PorN domains for T9SS assembly and effector recognition. Here we present the crystal structure of PorN at 2.0-Å resolution, which represents a novel fold with no significant similarity to any known structure. In agreement with *in silico* analyses, we also found that the N- and C-terminal regions of PorN are intrinsically disordered. Our functional studies showed that the N-terminal disordered region is involved in PorN dimerization while the C-terminal disordered region is involved in the interaction with PorK. Finally, we determined that the folded PorN central domain is involved in the interaction with PorM, as well as with the effector's CTD. Altogether, these results lay the foundations for a more comprehensive model of T9SS architecture and effector transport.**

Porphyromonas gingivalis, an anaerobic, nonmotile gram-negative bacterium, is the major human oral pathogen associated with periodontal diseases (1, 2). Chronic *P. gingivalis* infection is also linked to rheumatoid arthritis, heart disease, diabetes, Alzheimer disease, and other systemic diseases (3–9). Virulence factors responsible for *P. gingivalis* pathogenesis are secreted through the *Bacteroidetes*-specific type IX secretion system (T9SS) (10–12). These virulence factors are mainly cysteine proteases called gingipains that degrade host cell tissues and interfere with innate host defense mechanisms (13). Among other virulence factors secreted by the T9SS are the heme-binding protein Hbp35 involved in extracellular iron uptake (14) and the peptidylarginine deiminase PPAD whose citrullination activity is linked to rheumatoid arthritis (15). T9SS acts as a two-step mechanism: the substrate proteins are first exported into the periplasm by the Sec machinery after cleavage of their N-terminal signal peptide; then, a conserved C-terminal domain (CTD) is specifically recognized by the T9SS that transports them across the outer membrane (OM) (16, 17). Once outside the cell, the substrates are either delivered into the extracellular medium or remain attached to the cell surface through anchoring to anionic lipopolysaccharide (18–21).

Beside *P. gingivalis*, the T9SS is also encoded on the genome of a large subset of Bacteroidetes species, including the model bacterium *Flavobacterium johnsoniae* (10). In this nonpathogenic soil bacterium, the T9SS contributes to gliding motility by secreting SprB, a cell surface adhesin organized as filaments and that is required for movement on solid surfaces (22). Studies on *F. johnsoniae* motility led to the model that the T9SS is a new rotary machine driven by proton motive force powering SprB rotation (23).

To date, 18 genes have been identified as essential for T9SS function in *P. gingivalis* (12, 24). Among them, the *porK-L-M-N* genes (*gldK-L-M-N* in *F. johnsoniae*) are cotranscribed (25). The subunits encoded by these genes assemble into three subcomplexes: (i) a transenvelope complex comprising the PorK-L-M-N proteins; (ii) an OM-associated translocon complex through which effectors are transported across the OM and constituted of the Sov translocon, the plug protein, and PorV that is proposed to convey the effectors to (iii) the attachment complex, responsible for effector processing and attachment at the cell surface or release in the medium (12, 20). The PorK-L-M-N assembles as a >1.4-MDa complex that was proposed to constitute the T9SS core complex (26). This complex is proposed to select the effectors to be secreted via contacts between the effector CTDs and the PorM and PorN proteins (27). This core complex can be divided in two subcomplexes: the PorL-M inner membrane complex and the PorK-N OM-associated complex. PorL and PorM are both inner membrane proteins that interact through their

‡ These authors contributed equally to this work.
* For correspondence: Philippe Leone, philippe.leone@univ-amu.fr.

transmembrane helices (25). PorL has a cytoplasmic domain, whereas PorM harbors an extended periplasmic domain that spans most of the periplasmic space (28, 29). In *F. johnsoniae*, the GldL-M complex was proposed to be the rotary motor associated with gliding motility (30). Very recently, a partial structure of this complex was solved by cryo-EM, revealing a $GldL_5$-$GldM_2$ stoichiometry and demonstrating structural and functional homologies with known molecular motors (30).

The PorL-M complex interacts with the PorK-N OM-associated complex, through contacts between the PorM periplasmic domain and both PorN and PorK (25, 28). PorN is a periplasmic protein, whereas PorK is an OM lipoprotein (25). Cryo-EM and cryo-electron tomography observations revealed that the PorK-N complex assembles into large ring-shaped structures of 50 nm diameter (31, 32). These PorK-N rings are located in the periplasm, underneath the OM, and are proposed to be inserted into the OM by the PorK lipid moiety. These ring structures comprise approximately 32 to 36 subunits of each protein with a PorK:PorN molar ratio of 1:1. However, the resolution of the cryo-EM data was not sufficient to provide details on the structure of each partner, their organization into the ring, or their mode of interaction.

In this study, we focused on the PorN protein (PGN_1673; TIGR03523 family, GI: 188595217). *In silico* analyses and protease accessibility experiments suggested that the N- and C-terminal regions of PorN are intrinsically disordered. We further showed that these regions are involved in PorN oligomerization and PorK interaction. We then solved the structure of the PorN central core by X-ray crystallography, revealing a new fold, and showed that it mediates contacts with PorM and effector CTDs.

Results

PorN presents N- and C-terminal intrinsically disordered regions

In a previous study we have shown that the PorN periplasmic protein ($PorN_P$, residues 23–359, *i.e.*, devoid of the signal peptide) forms dimers and interacts with PorM and PorK (25). In order to get structural information, we overproduced and purified $PorN_P$ and carried out crystallization trials. Despite extensive screens, no crystal was obtained. Bioinformatic analysis of the PorN sequence suggested the presence of intrinsically disordered N- and C-terminal regions, which could prevent crystallization (Fig. 1). As intrinsically disordered regions are usually more prone to proteolysis, the $PorN_P$ protein preparation was subjected to limited proteolysis assay with different proteases, and a stable domain ($PorN_P$-G) was obtained after overnight incubation with the endoproteinase Glu-C at a 1:1000 (*w:w*) ratio (Fig. 2). Edman sequencing of $PorN_P$-G revealed that the protease-resistant folded domain starts at residue 55, and the molecular mass (24,949 Da) obtained by mass spectrometry suggested that it ends at residue 265.

The PorN N-terminal disordered region mediates dimer formation

The sequence encoding the PorN proteolysis-resistant fragment, $PorN_{\Delta N \Delta C}$ (residues 55–265), was cloned, and $PorN_{\Delta N \Delta C}$ was purified to homogeneity (Fig. 2). Size-exclusion chromatograpy–multiangle light scattering (SEC-MALS) analysis of $PorN_{\Delta N \Delta C}$ showed that the PorN folded core is monomeric, in contrast to the dimeric form of full-length PorN (Fig. 2). These results suggest that the N- and/or

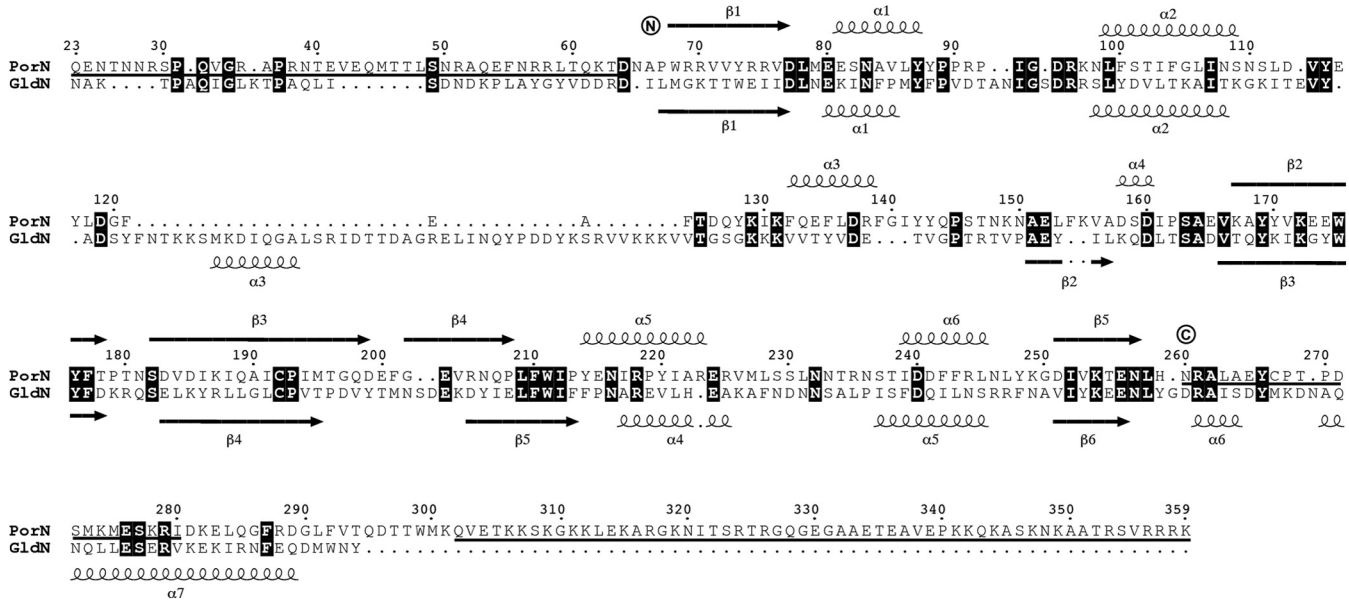

Figure 1. Sequence alignment of *P. gingivalis* PorN and *F. johnsoniae* GldN periplasmic proteins. PorN numbering is indicated on *top*, and secondary structures as observed in the crystal structure, are shown above the alignment; intrinsically disordered regions predicted by IUPred2A (51) are *underlined*; N and C termini of the $PorN_{\Delta N \Delta C}$ structure are indicated by the *circled* N and C, respectively. GldN secondary structures predicted by JPred4 (52) are displayed below the alignment. Amino acid sequences were aligned using T-Coffee (version 11.00.d625267, http://www.tcoffee.org) (53), and the figure was prepared using ESPript (version 3.0, http://espript.ibcp.fr/) (54).

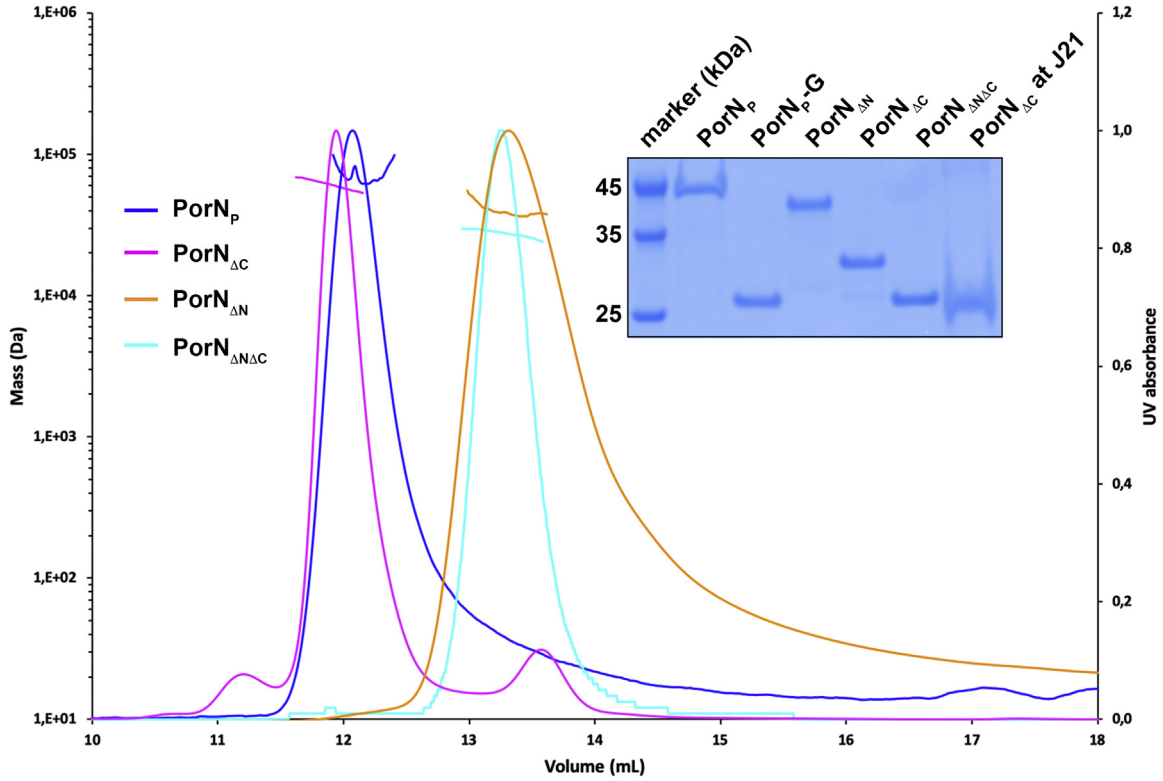

Figure 2. Size-exclusion chromatography–multiangle light scattering analysis of different PorN constructs. Chromatograms of purified PorN$_P$ (*blue*), PorN$_{\Delta N}$ (*orange*), PorN$_{\Delta C}$ (*magenta*), and PorN$_{\Delta N\Delta C}$ (*cyan*) are shown. The measured molar masses are ~82.1, ~38.8, ~61.7, and ~28.0 kDa for PorN$_P$, PorN$_{\Delta N}$, PorN$_{\Delta C}$, and PorN$_{\Delta N\Delta C}$, respectively. The *inset* shows the SDS-PAGE/Coomassie blue staining analysis of the different constructs.

C-terminal region(s) is/are involved in PorN$_P$ dimer formation. To better understand the contribution of the N- and C-terminal regions to PorN oligomerization, we engineered PorN$_P$ constructs deleted of the N- (PorN$_{\Delta N}$, residues 55–359), C- (PorN$_{\Delta C}$, residues 25–265), or both (PorN$_{\Delta N\Delta C}$, residues 55–265) terminal regions. These PorN variants were fused to the T18 and T25 domains of the adenylate cyclase, and pairwise interactions were tested by bacterial two-hybrid (BACTH) analyses. Our results show that PorN$_P$ and PorN$_{\Delta C}$ oligomerize but not PorN$_{\Delta N}$ or PorN$_{\Delta N\Delta C}$ (Fig. 3*A*), suggesting that the N-terminal region is required for PorN oligomerization. This result was confirmed *in vitro*. The different PorN constructs, fused to an N-terminal His$_6$ tag, were purified by metal affinity chromatography and gel filtration and subjected to SEC-MALS experiments. Figure 2 shows that PorN$_P$ and PorN$_{\Delta C}$ are dimeric in solution, whereas,

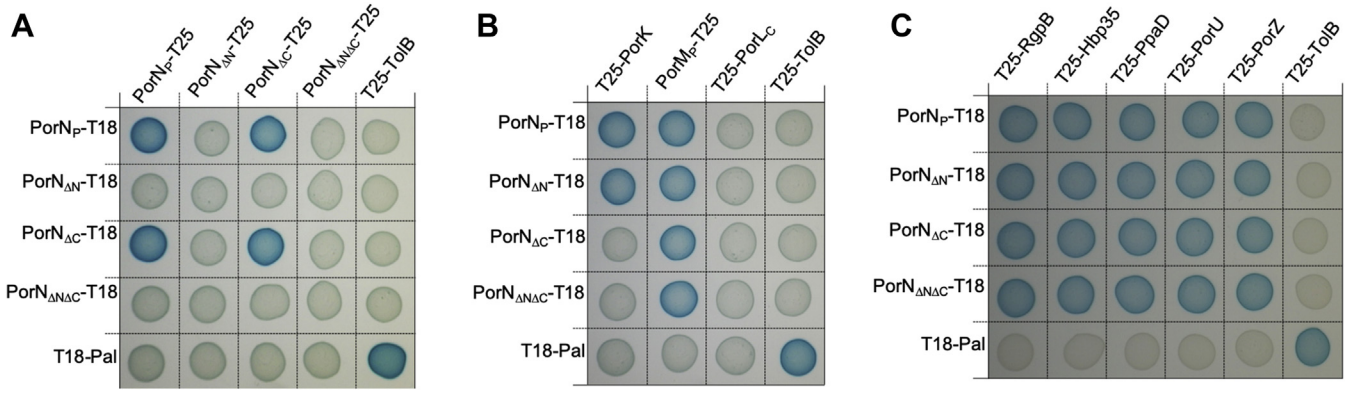

Figure 3. Bacterial two-hybrid analysis. Interaction of PorN variants with (*A*) themselves, (*B*) components of the PorKLMN complex, and (*C*) C-terminal secretion signals of T9SS effectors. BTH101 reporter cells producing the indicated proteins or domains fused to the T18 or T25 domain of the *Bordetella* adenylate cyclase were spotted on X-Gal-IPTG reporter LB agar plates. The *blue color* of the colony reports interaction between the two partners. Controls include T18 and T25 fusions to TolB and Pal, two proteins that interact but are unrelated to the T9SS. The assay has been performed in triplicate with identical results, and a representative experiment is shown. The different PorN domains are the entire periplasmic domain (PorN$_P$) and constructs deleted of the N-, or C-, or both terminal domains (PorN$_{\Delta N}$, PorN$_{\Delta C}$, and PorN$_{\Delta N\Delta C}$, respectively); PorK, soluble, unacylated form of PorK; PorM$_P$, PorM periplasmic domain; PorL$_C$, PorL cytosolic domain; RgpB, Hbp35, PPAD, PorU, PorZ, C-terminal domains of *P. gingivalis* gingipain RgpB, hemin-binding protein Hbp35, peptidylarginine deiminase PPAD, and T9SS components PorU and PorZ, respectively.

similarly to $PorN_{\Delta N\Delta C}$, $PorN_{\Delta N}$ is monomeric (Fig. 2). Taken together, the *in vivo* and *in vitro* assays demonstrate that PorN dimer formation is mediated by the N-terminal intrinsically disordered region.

Contributions of disordered regions and folded core to PorN interactions

PorN was previously shown to interact with the PorK OM lipoprotein, the PorM periplasmic domain, as well as the T9SS effector CTDs (25–27, 31). To gain information on the role of the N- and C-terminal disordered regions and of the central folded core, the PorN variants were assayed for their capacity to interact with PorK, PorM, and effector CTDs by BACTH. The unacylated form of PorK, the PorM periplasmic domain ($PorM_P$), the PorL cytoplasmic domain ($PorL_C$), and the CTDs of various T9SS substrates (the gingipain RgpB, the hemin-binding protein Hbp35, the peptidylarginine deiminase PPAD, and the T9SS components PorU and PorZ) were fused to the T25 domain and tested against T18-PorN fusions. Figure 3*B* shows that $PorN_P$ and $PorN_{\Delta N}$ interact with PorK and $PorM_P$, whereas $PorN_{\Delta C}$ interacts only with $PorM_P$. In addition, all PorN constructs interact with the CTDs of T9SS substrates (Fig. 3*C*). These results demonstrate that the PorN C-terminal disordered region is required for the interaction with PorK, whereas the PorN central core is sufficient to mediate contacts with PorM and the CTDs.

Crystal structure of the PorN central folded core

As described above, trials to crystallize $PorN_P$ were unsuccessful, probably because of the presence of N- and C-terminal intrinsically disordered regions. Crystallization trials were thus carried out with the $PorN_{\Delta N\Delta C}$ fragment, corresponding to the proteolysis-resistant fragment $PorN_P$-G. Selenomethionine (SeMet)-substituted $PorN_{\Delta N\Delta C}$ was purified and crystallized, and a single wavelength anomalous dispersion data set was collected at 2.5-Å resolution. Phases were calculated and an initial model comprising residues 67 to 258 was built. Two molecules are present in the asymmetric unit (Fig. S1), but this oligomerization state was likely induced by crystallization as SEC-MALS and BACTH analyses showed that $PorN_{\Delta N\Delta C}$ is monomeric (Figs. 2 and 3*A*). However, whether the arrangement of the two PorN molecules in the crystal packing corresponds to a physiological organization, or not, remains to be determined. In parallel, crystallization trials of the $PorN_{\Delta C}$ and $PorN_{\Delta N}$ fragments were performed. Only crystals of $PorN_{\Delta C}$ were obtained; they were isomorphous to those of $PorN_{\Delta N\Delta C}$, and a native data set was collected at 2.0-Å resolution. The model of $PorN_{\Delta N\Delta C}$ was used to solve the structure of $PorN_{\Delta C}$ by molecular replacement. Two molecules are present in the asymmetric unit, with the same orientation as $PorN_{\Delta N\Delta C}$. The superimposition of $PorN_{\Delta C}$ and $PorN_{\Delta N\Delta C}$ shows an r.m.s.d. of 0.94 Å, indicating that the two molecules are almost identical (Fig. S2). As expected, the N-terminal disordered region of $PorN_{\Delta C}$ is not visible in the electron density and the refined structure of $PorN_{\Delta C}$ comprises residues 66 to 260. Nevertheless, the presence of the missing residues is not compatible with the crystal packing, suggesting that $PorN_{\Delta C}$ has undergone proteolysis during crystallization. Indeed, SDS-PAGE analysis of purified $PorN_{\Delta C}$ confirmed that the protein was cleaved after 21 days, which corresponds to the crystal growth, and the size of the proteolytic product corresponds to that of $PorN_{\Delta N\Delta C}$ (Fig. 2).

The structure of the PorN folded core consists of an elongated antiparallel β-sheet covered on one side by six short α-helices connected by long loops, with connectivity β1α1α2α3α4β2β3β4α5α6β5 (Fig. 4). The β-sheet is composed of four β-strands on one extremity and two β-strands on the other, with the long 18-residue β-strand β3 being common to the two parts of the β-sheet. The N and C termini of the PorN folded domain are located very close to each other (<10 Å), suggesting that the N- and C-terminal disordered domains are likely to be at close proximity.

A structural similarity search within the Protein Data Bank (PDB) of the PorN folded domain structure using the DALI server (33) did not return any hit with statistically significant similarities. The highest Z-score (4.9) corresponds to the outer membrane enzyme PagL from *Pseudomonas aeruginosa* (PDB entry 2ERV), which folds into an eight-stranded β-barrel. Four β-strands of the PagL β-barrel superimpose with the four-stranded part of the PorN β-sheet with a core r.m.s.d. of 3.3 Á (Fig. S3). Actually, only the PorN β-sheet can be partially

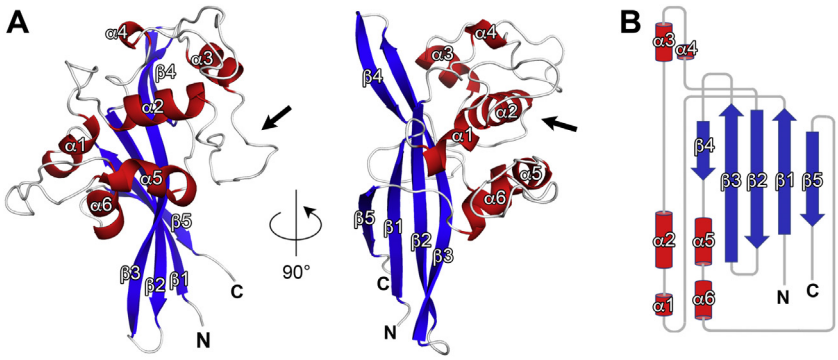

Figure 4. Overall structure of the *P. gingivalis* PorN folded domain. *A*, the PorN folded domain is shown as a *ribbon* diagram with *red* α-helices and *blue* β-sheets. The positions of the N and C termini are indicated. The figure was prepared using PyMOL (version 1.20, https://pymol.org). The position of the insertion (extra loop) in *F. johnsoniae* GldN is indicated by the *arrow*. *B*, topology diagram of *P. gingivalis* PorN. The figure was prepared using the TopScan plugin in PyMOL.

superimposed to a part of the structures corresponding to the 10 highest Z-score returned by the DALI server. This absence of similarity with any known structure suggests that the PorN core domain represents a new fold.

Discussion

The T9SS is a large multiprotein complex that delivers substrate proteins into the medium or that anchors them to the cell surface (2, 11, 20, 24). The recent years have started to provide information onto T9SS composition and organization, and the structures of some T9SS subunits have been solved. Here, we pursued this effort and report the structure–function analysis of the *P. gingivalis* PorN periplasmic protein. Together with PorK, PorN assembles large ring-shaped structures located underneath the membrane for which a low-resolution EM structure has been reported (31). Our analyses show that the PorN N- and C-terminal regions are intrinsically disordered, whereas the central domain is folded. The structure of the folded domain was then solved by X-ray crystallography and presents no similarity with any known structure.

It was previously shown that PorN dimerizes (25); our bacterial two-hybrid and SEC-MALS analyses reveal that dimerization is mediated by the N-terminal region. PorN dimerization is likely to be physiologically relevant, as PorN dimers were identified by chemical cross-linking of whole cells (31). Of interest, it was shown that a PorK-N ring is composed of 32 to 36 PorK-N complexes (31), suggesting that 16 to 18 PorN dimers are involved in ring formation. Bacterial two-hybrid assays revealed also the contribution of the other PorN domains for interaction with its partners. The C-terminal domain is involved in the interaction with PorK, while the folded domain is involved in the interaction with the periplasmic domain of PorM. Furthermore, we showed that the PorN folded domain is also involved in the interaction with the CTDs from five T9SS substrates, RgpB, Hbp35, PPAD, PorU, and PorZ. The current model of T9SS substrate transport suggests that substrates are selected in the periplasm by the PorM subunit and then conveyed to the OM-associated Sov translocon for their secretion across the OM. The PorKN ring, located underneath the OM, connects the PorM transenvelope protein to the translocon complex. By interacting with T9SS effectors, our results suggest that, in addition to playing a central role in the T9SS assembly, PorN is also involved in the trafficking of the substrates. We propose that the PorKN ring collects the effectors from the PorLM energetic module and provides them to the translocon.

It is interesting to note that PorN and its homologue in *F. johnsoniae*, GldN, differ significantly. Indeed, a sequence alignment between *P. gingivalis* PorN and *F. johnsoniae* GldN shows that no intrinsically disordered domains are predicted at the GldN C terminus (Fig. 1). Compared with PorN, the GldN folded domain is longer at its C terminus with two extra α-helices. However, an ∼40-amino acid–long insertion is present after helix α2 in GldN. Therefore, the GldN and PorN topologies are slightly different and, hence, the mode of binding to GldK might be different as the C-terminal disordered domain is not present in GldN. This raises the question as whether these potential structural differences between PorN and GldN could reveal differences in the assembly of the T9SS core complex in the two bacterial models *P. gingivalis* and *F. johnsoniae*. However, the GldN extra loop contains a significant proportion of charged residues (15/40), a characteristic shared with the PorN C-terminal region. Interesting, the position of this extra loop in the PorN structure showed that it is spatially located close to the C terminus, suggesting that the GldN extra loop and PorN C-terminal regions may play similar functions, such as interaction with GldK/PorK. Further investigations will be necessary to confirm that GldN interacts with GldK and whether this extra loop of GldN is involved in the interaction.

Experimental procedures

Strains, media growth conditions, and chemicals

Strains used in this study are listed in Table S1. *P. gingivalis* ATCC33277/DSMZ20709 was used as source of DNA for cloning. *P. gingivalis* was grown anaerobically in brain–heart infusion medium supplemented with menadiol (0.5 μg mL^{-1}) and hemin (5 μg mL^{-1}). *Escherichia coli* DH5α (New England Biolabs), BTH101 (34) and Rosetta (DE3) pLysS (Novagen) were used for cloning procedures, bacterial two-hybrid assays, and protein production, respectively. *E. coli* cells were routinely grown aerobically in Lysogeny broth (LB) at 30 °C or 37 °C. Plasmids were maintained by addition of ampicillin (100 μg mL^{-1}), kanamycin (50 μg mL^{-1}), or chloramphenicol (40 μg mL^{-1}).

Plasmid constructions

Plasmids and primers used for this study are listed in Table S1. The sequences encoding $PorN_P$ truncated of the N- or C- or both terminal domains ($PorN_{\Delta N}$ [residues 55–359], $PorN_{\Delta C}$ [residues 25–265], and $PorN_{\Delta N\Delta C}$ [residues 55–265], respectively) were amplified from *P. gingivalis* genomic DNA extracted from 6×10^9 cells using a DNA purification kit (DNeasy Blood & Tissue, Qiagen). PCRs were performed with a Biometra thermocycler using Q5 DNA polymerase (New England Biolabs) and custom oligonucleotides synthesized by Sigma-Aldrich (listed in Table S1).

For protein production, the sequences were cloned into pLIC03 (kindly provided by the BioXtal company, Marseille). The pLIC03 vector is a derivative of the pET28a+ expression vector (Novagen) in which a cassette coding for a His_6 tag and a tobacco etch virus protease cleavage site followed by the suicide gene *sacB* flanked by BsaI restriction sites was introduced downstream of the ATG start codon. The pLIC03 vector encoding the PorN periplasmic domain ($PorN_P$) has been described (25). pLIC03 vectors encoding truncated versions of PorN were engineered using the following primers: 5-$PorN_{\Delta N}$ and 3-$PorN_P$ (pLIC-$PorN_{\Delta N}$), 5-$PorN_P$ and 3-$PorN_{\Delta C}$ (pLIC-$PorN_{\Delta C}$), and 5-$PorN_{\Delta N}$ and 3-$PorN_{\Delta C}$ (pLIC-$PorN_{\Delta N\Delta C}$).

For bacterial two-hybrid assays, the sequences were cloned into pUT18C or pKT25 using the following primers:

T18T25-5-PorN$_{\Delta N}$ and T18C-3-PorN$_{\Delta N}$ (PorN$_{\Delta N}$ into pUT18C), T18T25-5-PorN$_{\Delta N}$ and T25C-3-PorN$_{\Delta N}$ (PorN$_{\Delta N}$ into pKT25), T25T18-5-PorN$_{\Delta C}$ and T18C-3-PorN$_{\Delta C}$ (PorN$_{\Delta C}$ into pUT18C), T25T18-5-PorN$_{\Delta C}$ and T25C-3-PorN$_{\Delta C}$ (PorN$_{\Delta C}$ into pKT25), T18T25-5-PorN$_{\Delta N}$ and T18C-3-PorN$_{\Delta C}$ (PorN$_{\Delta N\Delta C}$ into pUT18C), and T18T25-5-PorN$_{\Delta N}$ and T25C-3-PorN$_{\Delta C}$ (PorN$_{\Delta N\Delta C}$ into pKT25). BACTH vectors encoding PorN$_P$ (PorN periplasmic domain, residues 25–359) fused to the T18 domain, and PorK, PorL$_C$ (PorL cytoplasmic domain, amino acids 73–309), PorM$_P$ (PorM periplasmic domain, residues 36–516), and PorN$_P$ fused to the T25 domain have been described (25, 35). BACTH vectors encoding the C-terminal domains of RgpB (residues 661–736), Hbp35 (residues 226–344), PpaD (residues 478–557), PorU (residues 1059–1158), and PorZ (residues 680–776) fused to the T25 domain are described elsewhere (27).

Plasmids for protein production and for bacterial two-hybrid assays were engineered by restriction-free cloning (36), as described (37). Briefly, the DNA fragment of interest was amplified using oligonucleotides introducing extensions annealing to the target vector. The double-stranded product of the first PCR has then been used as oligonucleotides for a second PCR using the target vector (pLIC03, pUT18C, or pKT25) as template. PCR products were then treated with DpnI to eliminate template plasmids and transformed into DH5α-competent cells. All the constructs were verified by colony PCR and DNA sequencing (Eurofins sequencing).

Bacterial two-hybrid assay

Bordetella adenylate cyclase–based bacterial two-hybrid assays (34) were performed as described (38) with modifications. Briefly, the proteins to be tested were fused to the isolated T18 and T25 catalytic domains of the *Bordetella* adenylate cyclase. After introduction of the two plasmids expressing the fusion proteins into the reporter BTH101 strain, plates were incubated at 30 °C for 24 h. Three independent colonies for each transformation were inoculated into 600 µl of LB medium supplemented with ampicillin, kanamycin, and 0.5 mM IPTG. After overnight growth at 30 °C, 15 µl of each culture wase dropped onto LB plates supplemented with ampicillin, kanamycin, 0.5 mM IPTG, and 40 µg mL^{-1} X-Gal and incubated for 6 to 16 h at 30 °C. Controls included interaction assays with TolB/Pal, a protein pair unrelated to the T9SS (38). The experiments were done in triplicate, and a representative result is shown.

Protein production and purification

PorN$_P$, PorN$_{\Delta N}$, PorN$_{\Delta C}$, and PorN$_{\Delta N\Delta C}$ were produced as described (25) with modifications. Rosetta (DE3) pLysS *E. coli* cells were grown in Turbo Broth medium at 37 °C until reaching optical density at λ = 600 nm (A_{600nm}) of 0.6 to 0.8. Expression of the constructs was induced with 1 mM IPTG, and cells were grown for an additional 18 h at 17 °C. Cells were harvested by centrifugation at 4000*g* for 10 min, resuspended in lysis buffer (50 mM Tris-HCl pH 8.0, 300 mM NaCl, 10 mM imidazole, 250 µg mL^{-1} lysozyme, 1 mM PMSF), and frozen overnight at −20 °C. After thawing, 20 µg mL−^{1} DNase and 1 mM $MgSO_4$ were added, and cells were lysed by sonication. The pellet and soluble fractions were separated by centrifugation at 16,000*g* for 30 min, and the proteins were purified from the soluble fraction by immobilized metal ion affinity chromatography using a 5-ml HisTrap crude (GE Healthcare) Ni^{2+}-chelating column equilibrated in buffer A (50 mM Tris-HCl pH 8.0, 300 mM NaCl, 10 mM imidazole). The proteins were eluted with buffer A supplemented with 250 mM imidazole and further purified by size exclusion chromatography (HiLoad 16/60 Superdex 75 prep grade, GE Healthcare) equilibrated in 10 mM Hepes pH 7.5, 150 mM NaCl. SeMet-labeled PorN$_{\Delta N\Delta C}$ was produced and purified with the same protocol as the native proteins, except that the cells were grown in SeMet minimal medium (39).

For limited proteolysis assay, 15 µg of purified PorN$_P$ was incubated with 1:1000 (*w:w*) endoproteinase Glu-C (Thermo Fischer) for 16 h at 23 °C. After SDS-PAGE, the band corresponding to the stable Glu-C resistant fragment (PorN$_P$-G) was excised and analyzed by mass spectrometry and N-terminal Edman sequencing.

For SEC-MALS analysis, the purified PorN$_P$, (0.75 mg mL−^{1}), PorN$_{\Delta N}$ (0.7 mg mL−^{1}), PorN$_{\Delta C}$ (0.7 mg mL−^{1}), and PorN$_{\Delta N\Delta C}$ (1.4 mg mL^{-1}) proteins were loaded on a Superdex 200 Increase 10/300 GL column (GE Healthcare) equilibrated in 10 mM Hepes pH 7.4, 150 mM NaCl at a flow rate of 0.6 ml.min^{-1}, using an Ultimate 3000 HPLC system (Fischer Scientific). Detection was performed using an eight-angle light-scattering detector (DAWN8, Wyatt Technology) and a differential refractometer (Optilab, Wyatt Technology).

Crystallization, data collection, and processing

The purified PorN$_{\Delta C}$ and SeMet PorN$_{\Delta N\Delta C}$ were concentrated at 10.7 and 10.8 mg mL^{-1}, respectively. Crystallization trials were performed using the sitting-drop vapor-diffusion method at 293 K in 96-well Swissci-3 plates, with Stura Footprint (Molecular Dimensions), Wizard I and II (Rigaku), and Index (Hampton Research) screens and using Tecan and Mosquito (TTP Labtech) robots to fill in the plates and dispense the drops, respectively. Crystals were obtained in several conditions, and after optimization (40), the final crystallization conditions for PorN$_{\Delta C}$ and SeMet PorN$_{\Delta N\Delta C}$ were 33 mM Tris pH 8.5, 6.66% PEG 1000, 15.27% PEG 6000, 0.66 M citric acid pH 4.14, and 0.66 M Hepes pH 7.28, 3.2% PEG 3350, 10% glycerol, 3.3 mM $NiCl_2$ hexahydrate, respectively. Crystals were mounted in cryoloops (Hampton CrystalCap Magnetic) and were briefly soaked in crystallization solution supplemented with 24.7% PEG 6000, 6.66% PEG 8000 for PorN$_{\Delta C}$ and 31.3% PEG 3350, 6.6% glycerol for SeMet PorN$_{\Delta N\Delta C}$. The crystals were flash cooled in a nitrogen-gas stream at 100 K using a home cryocooling device (Oxford Cryosystems).

PorN$_{\Delta C}$ diffraction data were collected to 2-Å resolution on beamline ID30 at the European Synchrotron Research Facility (ESRF, Grenoble, France), and single wavelength anomalous

Table 1
Data collection and refinement statistics

	$PorN_{\Delta C}$	SeMet $PorN_{\Delta N\Delta C}$
Data collection		
Space group	$C222_1$	$C222_1$
a, b, c (Å)	47.7, 132.5, 133.7	47.9, 132.6, 136.4
α, β, γ (°)	90, 90, 90	90, 90, 90
Resolution (Å)[a]	47.0–2.0 (2.11–2.0)	40.0–2.5 (2.63–2.5)
Unique reflections[a]	28,600 (4169)	15,557 (2194)
Redundancy[a]	3.9 (4.0)	13.4 (13.6)
Completeness (%)[a]	98.3 (99.8)	99.7 (98.3)
I/σ[a]	11.1 (1.5)	16.5 (3.3)
R_{meas} (%)[a]	7.3 (102.6)	9.2 (74.2)
CC1/2	0.998 (0.610)	0.999 (0.761)
Mosaicity	0.09	0.12
Refinement and model quality		
Resolution (Å)[a]	42.5–2.0	
Reflections	28,568	
R_{fac}/R_{free} (%)	19.6/22.8	
Number of atoms		
Protein (chains in ASU)/water	1610 (2)/216	
B-factors ($Å^2$)		
Protein/water	57.9/56.0	
Rmsd		
Bond (Å)	0.009	
Angle (°)	0.94	
Ramachandran plot (%)		
Most favored	96.8	
Allowed regions	1.8	
Outliers	1.4	
PDB accession code	7PVH	

[a] Values in parentheses are for the highest-resolution shell.

dispersion data of SeMet $PorN_{\Delta N\Delta C}$ were collected to 2.5-Å resolution on beamline Proxima-2 at the Soleil synchrotron. The datasets were integrated with XDS (https://xds.mr.mpg.de/) (41) and scaled with SCALA (42) from the CCP4 suite (https://www.ccp4.ac.uk/) (43). Heavyatom substructure determination of SeMet $PorN_{\Delta N\Delta C}$, positional refinement, phase calculations, and solvent flattening were performed using autoSHARP (44), SHARP (45) and SOLOMON (46). The initial $PorN_{\Delta N\Delta C}$ model was built manually in COOT (47) and was subsequently used as model for molecular replacement with MOLREP (48) to solve the structure of native $PorN_{\Delta C}$. The building of $PorN_{\Delta C}$ was then completed manually with COOT. Refinement, correction, and validation of the structure were performed with autoBUSTER (49), COOT, and Molprobity (50), respectively. Data collection and refinement statistics are reported in Table 1.

Data availability

All details regarding PorN crystal structure (raw data from crystallography experiments, atomic coordinates, and structure factors) have been deposited in the PDB under accession code 7PVH.

Supporting information—This article contains supporting information (25, 27, 34, 38).

Acknowledgments—We thank the staff of the ESRF and Soleil synchrotrons for their assistance and for beamline allocation. We thank members of the Roussel and Cascales research groups for discussion and support.

Author contributions—E. C., A. R., and P. L. conceptualization; E. C. and P. L. methodology; E. C., A. R., and P. L. validation; O. F., I. L. S., E. C., and P. L. formal analysis; O. F., I. L. S., E. C., and P. L. investigation; P. L. writing – original draft; E. C. writing – review & editing; E. C., A. R., and P. L. supervision; E. C. and A. R. project administration; E. C. and A. R. funding acquisition.

Funding and additional information—This work was funded by the Centre National de la Recherche Scientifique, the Aix-Marseille Université, and grants from the Agence Nationale de la Recherche (ANR-15-CE11-0019 [to E. C.] and ANR-20-CE11-0011 [to P. L.]) and from the Excellence Initiative of Aix-Marseille Université, a French "Investissements d'Avenir" programme (A*MIDEX AAP-ID-17-33) to E. C. The PhD thesis of I. L. S. has been funded by the ANR-15-CE11-0019 grant.

Conflict of interest—The authors declare that they have no conflicts of interest with the contents of this article.

Abbreviations—The abbreviations used are: BACTH, bacterial two-hybrid; CTD, C-terminal domain; OM, outer membrane; PDB, protein data bank; SEC-MALS, size-exclusion chromatography–multiangle light scattering; SeMet, selenomethionine; T9SS, type IX secretion system.

References

1. Bostanci, N., and Belibasakis, G. N. (2012) *Porphyromonas gingivalis*: An invasive and evasive opportunistic oral pathogen. *FEMS Microbiol. Lett.* **333**, 1–9
2. Lunar Silva, I., and Cascales, E. (2021) Molecular strategies underlying *Porphyromonas gingivalis* virulence. *J. Mol. Biol.* **433**, 166836
3. Garcia, R. I., Henshaw, M. M., and Krall, E. A. (2001) Relationship between periodontal disease and systemic health. *Periodontol. 2000* **25**, 21–36
4. Bahekar, A. A., Singh, S., Saha, S., Molnar, J., and Arora, R. (2007) The prevalence and incidence of coronary heart disease is significantly increased in periodontitis: A meta-analysis. *Am. Heart J.* **154**, 830–837
5. Meyer, M. S., Joshipura, K., Giovannucci, E., and Michaud, D. S. (2008) A review of the relationship between tooth loss, periodontal disease, and cancer. *Cancer Causes Control* **19**, 895–907
6. Singhrao, S. K., Harding, A., Poole, S., Kesavalu, L., and Crean, S. (2015) *Porphyromonas gingivalis* periodontal infection and its putative links with Alzheimer's disease. *Mediators Inflamm.* **2015**, 1–10
7. Olsen, I., Singhrao, S. K., and Potempa, J. (2018) Citrullination as a plausible link to periodontitis, rheumatoid arthritis, atherosclerosis and Alzheimer's disease. *J. Oral Microbiol.* **10**, 1487742
8. Eriksson, K., Fei, G., Lundmark, A., Benchimol, D., Lee, L., Hu, Y. O. O., Kats, A., Saevarsdottir, S., Catrina, A. I., Klinge, B., Andersson, A. F., Klareskog, L., Lundberg, K., Jansson, L., and Yucel-Lindberg, T. (2019) Periodontal health and oral microbiota in patients with rheumatoid arthritis. *J. Clin. Med.* **8**, 630
9. Perricone, C., Ceccarelli, F., Matteo, S., Di Carlo, G., Bogdanos, D. P., Lucchetti, R., Pilloni, A., Valesini, G., Polimeni, A., and Conti, F. (2019) *Porphyromonas gingivalis* and rheumatoid arthritis. *Curr. Opin. Rheumatol.* **31**, 517–524
10. McBride, M. J., and Zhu, Y. (2013) Gliding motility and Por secretion system genes are widespread among members of the phylum *Bacteroidetes*. *J. Bacteriol.* **195**, 270–278
11. McBride, M. J. (2019) *Bacteroidetes* gliding motility and the type IX secretion system. *Microbiol. Spectr.* **7**. https://doi.org/10.1128/microbiolspec.PSIB-0002-2018
12. Gorasia, D. G., Veith, P. D., and Reynolds, E. C. (2020) The type IX secretion system: Advances in structure, function and organisation. *Microorganisms* **8**, 1173
13. Hajishengallis, G. (2015) Periodontitis: From microbial immune subversion to systemic inflammation. *Nat. Rev. Immunol.* **15**, 30–44

14. Shoji, M., Sato, K., Yukitake, H., Kondo, Y., Narita, Y., Kadowaki, T., Naito, M., and Nakayama, K. (2011) Por secretion system-dependent secretion and glycosylation of *Porphyromonas gingivalis* hemin-binding protein 35. *PLoS One* **6**, e21372
15. Montgomery, A. B., Kopec, J., Shrestha, L., Thezenas, M.-L., Burgess-Brown, N. A., Fischer, R., Yue, W. W., and Venables, P. J. (2016) Crystal structure of *Porphyromonas gingivalis* peptidylarginine deiminase: Implications for autoimmunity in rheumatoid arthritis. *Ann. Rheum. Dis.* **75**, 1255–1261
16. Seers, C. A., Slakeski, N., Veith, P. D., Nikolof, T., Chen, Y.-Y., Dashper, S. G., and Reynolds, E. C. (2006) The RgpB C-terminal domain has a role in attachment of RgpB to the outer membrane and belongs to a novel C-terminal-domain family found in *Porphyromonas gingivalis*. *J. Bacteriol.* **188**, 6376–6386
17. Veith, P. D., Nor Muhammad, N. A., Dashper, S. G., Likić, V. A., Gorasia, D. G., Chen, D., Byrne, S. J., Catmull, D. V., and Reynolds, E. C. (2013) Protein substrates of a novel secretion system are numerous in the *Bacteroidetes* phylum and have in common a cleavable C-terminal secretion signal, extensive post-translational modification, and cell-surface attachment. *J. Proteome Res.* **12**, 4449–4461
18. Glew, M. D., Veith, P. D., Peng, B., Chen, Y.-Y., Gorasia, D. G., Yang, Q., Slakeski, N., Chen, D., Moore, C., Crawford, S., and Reynolds, E. C. (2012) PG0026 is the C-terminal signal peptidase of a novel secretion system of *Porphyromonas gingivalis*. *J. Biol. Chem.* **287**, 24605–24617
19. Gorasia, D. G., Veith, P. D., Chen, D., Seers, C. A., Mitchell, H. A., Chen, Y.-Y., Glew, M. D., Dashper, S. G., and Reynolds, E. C. (2015) *Porphyromonas gingivalis* type IX secretion substrates are cleaved and modified by a sortase-like mechanism. *PLoS Pathog.* **11**, e1005152
20. Veith, P. D., Glew, M. D., Gorasia, D. G., and Reynolds, E. C. (2017) Type IX secretion: The generation of bacterial cell surface coatings involved in virulence, gliding motility and the degradation of complex biopolymers. *Mol. Microbiol.* **106**, 35–53
21. Madej, M., Nowakowska, Z., Ksiazek, M., Lasica, A. M., Mizgalska, D., Nowak, M., Jacula, A., Bzowska, M., Scavenius, C., Enghild, J. J., Aduse-Opoku, J., Curtis, M. A., Gomis-Rüth, F. X., and Potempa, J. (2021) PorZ, an essential component of the type IX secretion system of *Porphyromonas gingivalis*, delivers anionic lipopolysaccharide to the PorU sortase for transpeptidase processing of T9SS cargo proteins. *mBio* **12**, e02262-20
22. Nelson, S. S., Bollampalli, S., and McBride, M. J. (2008) SprB is a cell surface component of the *Flavobacterium johnsoniae* gliding motility machinery. *J. Bacteriol.* **190**, 2851–2857
23. Shrivastava, A., Lele, P. P., and Berg, H. C. (2015) A rotary motor drives *Flavobacterium* gliding. *Curr. Biol.* **25**, 338–341
24. Lasica, A. M., Ksiazek, M., Madej, M., and Potempa, J. (2017) The type IX secretion system (T9SS): Highlights and recent insights into its structure and function. *Front. Cell. Infect. Microbiol.* **7**, 215
25. Vincent, M. S., Canestrari, M. J., Leone, P., Stathopoulos, J., Ize, B., Zoued, A., Cambillau, C., Kellenberger, C., Roussel, A., and Cascales, E. (2017) Characterization of the *Porphyromonas gingivalis* type IX secretion trans-envelope PorKLMNP core complex. *J. Biol. Chem.* **292**, 3252–3261
26. Sato, K., Naito, M., Yukitake, H., Hirakawa, H., Shoji, M., McBride, M. J., Rhodes, R. G., and Nakayama, K. (2010) A protein secretion system linked to bacteroidete gliding motility and pathogenesis. *Proc. Natl. Acad. Sci. U. S. A.* **107**, 276–281
27. [preprint] Vincent, M. S., Chabalier, M., and Cascales, E. (2018) A conserved motif of *Porphyromonas* type IX secretion effectors C-terminal secretion signal specifies interactions with the PorKLMN core complex. *bioRxiv*. https://doi.org/10.1101/483123
28. Leone, P., Roche, J., Vincent, M. S., Tran, Q. H., Desmyter, A., Cascales, E., Kellenberger, C., Cambillau, C., and Roussel, A. (2018) Type IX secretion system PorM and gliding machinery GldM form arches spanning the periplasmic space. *Nat. Commun.* **9**, 429
29. Sato, K., Okada, K., Nakayama, K., and Imada, K. (2020) PorM, a core component of bacterial type IX secretion system, forms a dimer with a unique kinked-rod shape. *Biochem. Biophys. Res. Commun.* **532**, 114–119
30. Hennell James, R., Deme, J. C., Kjær, A., Alcock, F., Silale, A., Lauber, F., Johnson, S., Berks, B. C., and Lea, S. M. (2021) Structure and mechanism of the proton-driven motor that powers type 9 secretion and gliding motility. *Nat. Microbiol.* **6**, 221–233
31. Gorasia, D. G., Veith, P. D., Hanssen, E. G., Glew, M. D., Sato, K., Yukitake, H., Nakayama, K., and Reynolds, E. C. (2016) Structural insights into the PorK and PorN components of the *Porphyromonas gingivalis* type IX secretion system. *PLoS Pathog.* **12**, e1005820
32. [preprint] Gorasia, D. G., Chreifi, G., Seers, C. A., Butler, C. A., Heath, J. E., Glew, M. D., McBride, M. J., Subramanian, P., Kjær, A., Jensen, G. J., Veith, P. D., and Reynolds, E. C. (2020) *In situ* structure and organisation of the type IX secretion system. *bioRxiv*. https://doi.org/10.1101/2020.05.13.094771
33. Holm, L., and Rosenström, P. (2010) Dali server: Conservation mapping in 3D. *Nucleic Acids Res.* **38**, W545–W549
34. Karimova, G., Pidoux, J., Ullmann, A., and Ladant, D. (1998) A bacterial two-hybrid system based on a reconstituted signal transduction pathway. *Proc. Natl. Acad. Sci. U. S. A.* **95**, 5752–5756
35. Vincent, M. S., Durand, E., and Cascales, E. (2016) The PorX response regulator of the *Porphyromonas gingivalis* PorXY two-component system does not directly regulate the type IX secretion genes but binds the PorL subunit. *Front. Cell. Infect. Microbiol.* **6**, 96
36. van den Ent, F., and Lowe, J. (2006) RF cloning: A restriction-free method for inserting target genes into plasmids. *J. Biochem. Biophys. Methods* **67**, 67–74
37. Aschtgen, M.-S., Gavioli, M., Dessen, A., Lloubès, R., and Cascales, E. (2010) The SciZ protein anchors the enteroaggregative *Escherichia coli* type VI secretion system to the cell wall. *Mol. Microbiol.* **75**, 886–899
38. Battesti, A., and Bouveret, E. (2012) The bacterial two-hybrid system based on adenylate cyclase reconstitution in Escherichia coli. *Methods* **58**, 325–334
39. Guerrero, S. A., Hecht, H. J., Hofmann, B., Biebl, H., and Singh, M. (2001) Production of selenomethionine-labelled proteins using simplified culture conditions and generally applicable host/vector systems. *Appl. Microbiol. Biotechnol.* **56**, 718–723
40. Lartigue, A., Gruez, A., Briand, L., Pernollet, J.-C., Spinelli, S., Tegoni, M., and Cambillau, C. (2003) Optimization of crystals from nanodrops: Crystallization and preliminary crystallographic study of a pheromone-binding protein from the honeybee *Apis mellifera L. Acta Crystallogr. D Biol. Crystallogr.* **59**, 919–921
41. Kabsch, W. (2010) Integration, scaling, space-group assignment and post-refinement. *Acta Crystallogr. D Biol. Crystallogr.* **66**, 133–144
42. Evans, P. (2006) Scaling and assessment of data quality. *Acta Crystallogr. D Biol. Crystallogr.* **62**, 72–82
43. Collaborative Computational Project, Number 4 (1994) The CCP4 suite: Programs for protein crystallography. *Acta Crystallogr. D Biol. Crystallogr.* **50**, 760–763
44. Vonrhein, C., Blanc, E., Roversi, P., and Bricogne, G. (2007) Automated structure solution with autoSHARP. *Methods Mol. Biol.* **364**, 215–230
45. Bricogne, G., Vonrhein, C., Flensburg, C., Schiltz, M., and Paciorek, W. (2003) Generation, representation and flow of phase information in structure determination: Recent developments in and around SHARP 2.0. *Acta Crystallogr. D Biol. Crystallogr.* **59**, 2023–2030
46. Abrahams, J. P., and Leslie, A. G. (1996) Methods used in the structure determination of bovine mitochondrial F1 ATPase. *Acta Crystallogr. D Biol. Crystallogr.* **52**, 30–42
47. Emsley, P., and Cowtan, K. (2004) Coot: Model-building tools for molecular graphics. *Acta Crystallogr. D Biol. Crystallogr.* **60**, 2126–2132
48. Vagin, A., and Teplyakov, A. (2010) Molecular replacement with MOLREP. *Acta Crystallogr. D Biol. Crystallogr.* **66**, 22–25
49. Blanc, E., Roversi, P., Vonrhein, C., Flensburg, C., Lea, S. M., and Bricogne, G. (2004) Refinement of severely incomplete structures with maximum likelihood in BUSTER-TNT. *Acta Crystallogr. D Biol. Crystallogr.* **60**, 2210–2221
50. Chen, V. B., Arendall, W. B., Headd, J. J., Keedy, D. A., Immormino, R. M., Kapral, G. J., Murray, L. W., Richardson, J. S., and

Richardson, D. C. (2010) *MolProbity* : All-atom structure validation for macromolecular crystallography. *Acta Crystallogr. D Biol. Crystallogr.* **66**, 12–21
51. Erdős, G., and Dosztányi, Z. (2020) Analyzing protein disorder with IUPred2A. *Curr. Protoc. Bioinformatics* **70**, e99
52. Drozdetskiy, A., Cole, C., Procter, J., and Barton, G. J. (2015) JPred4: A protein secondary structure prediction server. *Nucleic Acids Res.* **43**, W389–W394
53. Di Tommaso, P., Moretti, S., Xenarios, I., Orobitg, M., Montanyola, A., Chang, J.-M., Taly, J.-F., and Notredame, C. (2011) T-coffee: A web server for the multiple sequence alignment of protein and RNA sequences using structural information and homology extension. *Nucleic Acids Res.* **39**, W13–W17
54. Robert, X., and Gouet, P. (2014) Deciphering key features in protein structures with the new ENDscript server. *Nucleic Acids Res.* **42**, W320–W324